Radiology

ORIGINAL RESEARCH • NEUROradiology

World Health Organization Grade II/III Glioma Molecular Status: Prediction by MRI Morphologic Features and Apparent Diffusion Coefficient

*John Maynard, FRCR** • *Sachi Okuchi, PhD** • *Stephen Wastling, PhD* • *Ayisha Al Busaidi, FRCR* • *Ofran Almossawi, MSc* • *Wonderboy Mbatha, MD* • *Sebastian Brandner, FRCPath, PhD* • *Zane Jaunmuktane, FRCPath, MD* • *Ali Murat Koc, MD* • *Laura Mancini, PhD* • *Rolf Jäger, MD, FRCR* • *Stefanie Thust, MD, FRCR*

From the Neuroradiological Academic Unit, Department of Brain, Repair and Rehabilitation, UCL Institute of Neurology, London, England (J.M., S.O., S.W., L.M., R.J., S.T.); Lysholm Department of Neuroradiology, National Hospital for Neurology and Neurosurgery, Queen Square, London WC1N 3BG, England (S.W., A.A.B., W.M., A.M.K., L.M., R.J., S.T.); Population, Policy and Practice Research Unit, UCL Great Ormond Street Institute of Child Health, London, England (O.A.); Department of Neurodegenerative Disease, UCL Institute of Neurology and Division of Neuropathology, National Hospital for Neurology and Neurosurgery, London, England (S.B., Z.J.); and Department of Imaging, University College London Foundation Hospital, London, England (R.J., S.T.); Received August 15, 2019; revision requested October 1; revision received January 21, 2020; accepted February 10. **Address correspondence to** S.T. (e-mail: *s.thust@ucl.ac.uk*).

This study originates from University College London Hospitals, which receives a proportion of funding from the National Institute of Health Research Biomedical Research Centre.

* J.M. and S.O. contributed equally to this work.

Conflicts of interest are listed at the end of this article.

Radiology 2020; 00:1–10 • https://doi.org/10.1148/radiol.2020191832 • Content codes: NR MR

Background: A readily implemented MRI biomarker for glioma genotyping is currently lacking.

Purpose: To evaluate clinically available MRI parameters for predicting isocitrate dehydrogenase (*IDH*) status in patients with glioma.

Materials and Methods: In this retrospective study of patients studied from July 2008 to February 2019, untreated World Health Organization (WHO) grade II/III gliomas were analyzed by three neuroradiologists blinded to tissue results. Apparent diffusion coefficient (ADC) minimum (ADC_{min}) and mean (ADC_{mean}) regions of interest were defined in tumor and normal appearing white matter (ADC_{NAWM}). A visual rating of anatomic features (T1 weighted, T1 weighted with contrast enhancement, T2 weighted, and fluid-attenuated inversion recovery) was performed. Interobserver comparison (intraclass correlation coefficient and Cohen κ) was followed by nonparametric (Kruskal-Wallis analysis of variance) testing of associations between ADC metrics and glioma genotypes, including Bonferroni correction for multiple testing. Descriptors with sufficient concordance (intraclass correlation coefficient, >0.8; $\kappa > 0.6$) underwent univariable analysis. Predictive variables ($P < .05$) were entered into a multivariable logistic regression and tested in an additional test sample of patients with glioma.

Results: The study included 290 patients (median age, 40 years; interquartile range, 33–52 years; 169 male patients) with 82 *IDH* wild-type, 107 *IDH* mutant/1p19q intact, and 101 *IDH* mutant/1p19q codeleted gliomas. Two predictive models incorporating ADC_{mean}-to-ADC_{NAWM} ratio, age, and morphologic characteristics, with model A mandating calcification result and model B recording cyst formation, classified tumor type with areas under the receiver operating characteristic curve of 0.94 (95% confidence interval [CI]: 0.91, 0.97) and 0.96 (95% CI: 0.93, 0.98), respectively. In the test sample of 49 gliomas (nine *IDH* wild type, 21 *IDH* mutant/*1p19q* intact, and 19 *IDH* mutant/*1p19q* codeleted), the classification accuracy was 40 of 49 gliomas (82%; 95% CI: 71%, 92%) for model A and 42 of 49 gliomas (86%; 95% CI: 76%, 96%) for model B.

Conclusion: Two algorithms that incorporated apparent diffusion coefficient values, age, and tumor morphologic characteristics predicted isocitrate dehydrogenase status in World Health Organization grade II/III gliomas on the basis of standard clinical MRI sequences alone.

Online supplemental material is available for this article.

A subgroup of lower-grade gliomas is characterized by genetic overlap with primary glioblastoma and exhibits similarly rapid disease progression (1,2). Such malignant neoplasms are indistinguishable from indolent astrocytomas by assessing proliferative indexes and cell morphologic features (3). Mutations in the isocitrate dehydrogenase (*IDH*) gene, most commonly *IDH1* (*R132H*), define most slow-growing gliomas (>70%) within the World Health Organization (WHO) histologic grades II/III (4). *IDH* mutations (IDH^{mut}) are absent (*IDH* wild-type [IDH^{wt}]) in lower-grade tumors of the primary glioblastoma spectrum, which further differ by genetic hallmarks of combined chromosome-7 gain and chromosome-10 loss, epidermal growth factor receptor amplification, and telomerase reverse transcriptase promoter mutations (2). Among IDH^{mut} gliomas, synchronous deletion of the short arm of chromosome 1 and long arm of chromosome 19 ($IDH^{mut}/1p19q^{del}$) constitutes a specific feature of oligodendrogliomas, whereas IDH^{mut} astrocytomas are mostly *1p19q* intact ($IDH^{mut}/1p19q^{int}$) (5). This genetic grouping serves an important clinical purpose of stratifying tumors with differential susceptibility to adjuvant treatment; for example, $IDH^{mut}/1p19q^{del}$ gliomas have greater sensitivity to alkylating chemotherapy (6).

Abbreviations

ADC = apparent diffusion coefficient, ADC_{mean} = mean ADC, ADC_{min} = minimum ADC, ADC_{NAWM} = ADC in normal-appearing white matter, AUC = area under the receiver operating characteristic curve, CI = confidence interval, FLAIR = fluid-attenuated inversion recovery, *IDH* = isocitrate dehydrogenase, IDH^{mut} = *IDH* mutation, IDH^{wt} = *IDH* wild-type, ROI = region of interest, WHO = World Health Organization

Summary

An algorithm on the basis of standard MRI sequences and age predicted isocitrate dehydrogenase status in lower-grade gliomas without advanced computational methods.

Key Results

- Apparent diffusion coefficient (ADC) measurements supported the distinction of nongadolinium chelate–enhancing and solid enhancing lower-grade glioma genotypes ($P < .001$).
- Glioma location, enhancement characteristics, calcification, and cyst formation were multivariable predictors of isocitrate dehydrogenase (*IDH*) status.
- Two predictive models incorporating ADC, age, and morphologic characteristics defined *IDH* genotype with accuracies of 92% and 91%.

Glioblastoma outcomes are improved with gross total gadolinium-based contrast agent–enhancing lesion resection (7) and potentially beyond this for T2 fluid-attenuated inversion recovery (FLAIR) component removal (8). The similarity between the biology of low-grade IDH^{wt} glioma and glioblastoma makes it crucial to identify glioblastoma early and separate it from the more favorable IDH^{mut} entities.

Diffusion-weighted MRI imaging is routinely used in cancer imaging. It functions on the assumption that free water motion in tissues diminishes with growing tumor cellularity (9). Three-direction diffusion-weighted imaging is widely performed and integrated into clinical glioma imaging protocols, and quantitative results are available immediately at reporting (10). Diffusion-based methods can support grading and have shown capability for *IDH* typing (11–13), including for gliomas in which there is no contrast enhancement (14). Prior studies (15) suggest that lesion properties such as location, internal architecture, and enhancement patterns differ between glioma genetic subtypes. Additionally, consideration of patient age may help diagnosis because it has been shown that IDH^{wt} gliomas are more common in older patients (16). The purpose of our study was to evaluate clinically available MRI parameters for predicting *IDH* status in patients with glioma.

Materials and Methods

Ethics review board approval was obtained and written informed consent was waived for this retrospective study.

Patient Cohort

All patients consecutively diagnosed with WHO grade II/III glioma at our national brain tumor referral institution between July 2008 and January 2018 were eligible for the study. Inclusion criteria were a proven histologic diagnosis of WHO grade II/III glioma, available *IDH* and *1p19q* genetic test results, and MRI examination before treatment.

Exclusion criteria included previous treatment for glioma; a tumor other than WHO grade II/III glioma; missing, inconclusive, or ambiguous molecular results (eg, IDH^{wt}/$1p19q^{del}$); prolonged (≥1 year) interval from MRI to operation; or missing images. In 44 of the 290 patients who were included, mean apparent diffusion coefficient (ADC; ADC_{mean}) values were reported in a previous study (14) that compared volumetric and regional ADC_{mean} measurements. In our study, multiple region-derived ADC metrics and morphologic descriptors were analyzed (by different observers) in these patients. Results derived from the original patient cohort (July 2008 to January 2018) were validated by using a previously unseen test sample of patients included between January 2018 and February 2019 (49 patients).

MRI Parameters

All MRI examinations included T2-weighted, T2-weighted FLAIR, and T1-weighted sequences before and after administration of a gadolinium-based contrast agent and diffusion-weighted imaging (211 examinations at 1.5 T and 79 examinations at 3.0 T). Our institution is a quaternary center and therefore the MRI examinations originated from multiple sites and systems (57 GE systems, 206 Siemens systems, 26 Phillips systems, and one Toshiba system). No machine model contributed more than 14% gliomas of one molecular subtype. The range of MRI parameters is provided in Table E1 (online).

Histopathologic Analysis

All tissue samples were fixed as paraffin blocks and analyzed at our institution's neuropathology department by using the latest method consistent with the WHO 2016 guidance on histopathologic analysis and immunohistochemistry (17). For *IDH R132H*–negative tumors, multiple-gene Sanger sequencing was performed to identify alternative *IDH* mutations. A quantitative polymerase chain reaction–based copy number assay was employed to determine 1p/19q status.

ADC Quantification

The ADC measurements were blinded to tissue diagnosis (reference standard), age, and other observers' results. Three independent observers (M.K., with 6 years of experience, and W.M., with 3 years of experience, both board-certified neuroradiologists; and S.O., a resident in training) placed three different 30–40-mm^2 regions of interest (ROIs) into the visually perceived lowest ADC portions of each glioma. From these, the mean value of the numerically lowest ADC ROI measurement was designated as the ADC minimum (ADC_{min}) as in Xing et al (11). Subsequently, one large ROI (ADC_{mean}) was drawn to cover the largest axial tumor cross-section, excluding tumor margins, necrosis, macroscopic hemorrhage, and calcifications. A comparative ADC ROI was placed in the normal-appearing white matter (ADC_{NAWM}), following a previous study (14), amounting to five ROIs per patient. Multifocal tumors were measured as one glioma. Observer 1 analyzed all 290 gliomas, observer 2 reanalyzed 75 gliomas, and observer 3 reanalyzed the remaining 215 gliomas, amounting to a

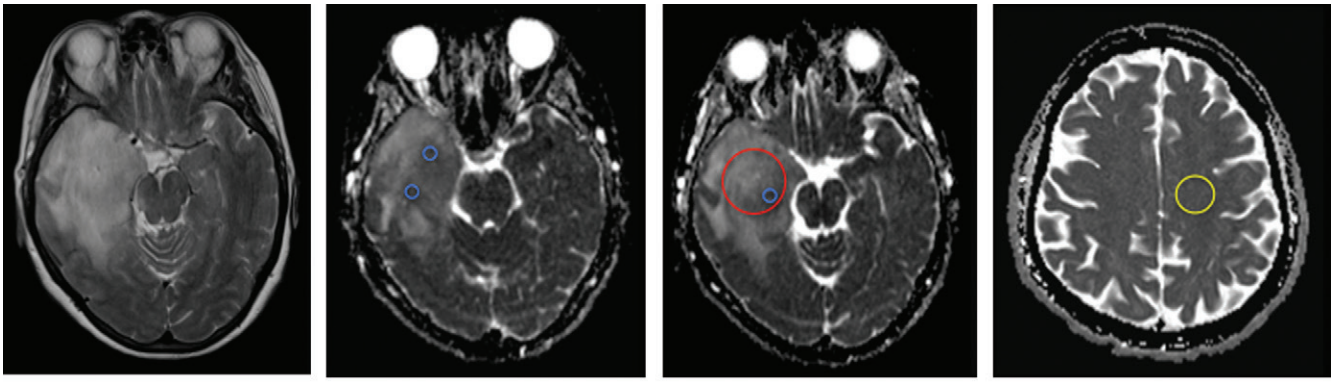

Figure 1: An example of apparent diffusion coefficient (ADC) measurements. **(a)** Axial T2-weighted image of a right temporal isocitrate dehydrogenase (*IDH*) wild-type glioma and **(b–d)** ADC maps showing the regions of interest used to determine minimum ADC (perceived lowest ADC regions [three per patient] blue), mean ADC (largest tumor cross-section measurement, red), and ADC in normal-appearing white matter (contralateral centrum semiovale, yellow). Note that round regions of interest were chosen because this method can be replicated on most picture archiving and communication systems.

total of 2900 ADC measurements. From these, ADC_{min}-to-ADC_{NAWM} and ADC_{mean}-to-ADC_{NAWM} ratios were calculated, resulting in four ADC parameters (ADC_{min}, ADC_{min}-to-ADC_{NAWM} ratio, ADC_{mean}, and ADC_{mean}-to-ADC_{NAWM} ratio) per patient.

For the test sample (n = 49), one researcher newly trained in the ADC method (A.A.B., a board-certified neuroradiologist with 3 years of experience) obtained all ADC values blinded as described. Figure 1 shows examples of the region placements.

Morphologic Assessment

Three observers (S.T., with 8 years of experience, and A.A.B., both board-certified neuroradiologists; and S.O., a resident) independently reviewed 290 MRI data sets and were blinded to diagnosis and the results of other observers. Morphologic readings were performed at a separate time (>2 weeks later than evaluation of ADC measurements). Feature categories were adapted on the basis of previous publications (16,18). Tumor location was specified by epicenter, with locations grouped according to the frequency of IDH^{wt} status to reduce the number of variables for statistical analysis. Multifocality was marked positive if more than one discrete tumor deposit was visible or if three or more lobes were involved. The nonenhancing tumor margin was described by using a visual rating scale as follows: 1, able to clearly draw around the lesion on T2-weighted images; to 4, indistinct margin on T2-weighted and FLAIR images. Hemorrhage and calcification were assessed at T1-weighted imaging together with CT, T2* sequences, and susceptibility-weighted imaging, as available. The option *uncertain* was added for these categories to allow for variability in the diagnostic sequences. The single largest tumor diameter was measured on T2-weighted images according to Pignatti et al (19). Contrast agent uptake was categorized into nonenhancing, patchy or solid, or rim enhancing. Rim enhancement surrounding central necrosis was distinguished from cysts, defined as exhibiting fluid signal isointense to cerebrospinal fluid with absent or minimal rim enhancement. T2-weighted FLAIR mismatch was specified according to Patel et al (20). Examples of different morphologic features of gliomas are shown in Figure 2.

Statistical Analysis

Statistical testing was performed by using software (SPSS 25, IBM, Armonk, NY; and Stata 15, Statacorp, College Station, Tex). The concordance of ADC measurements between observers was examined by intraclass correlation coefficient analysis, with a two-way random-effects model. For each ADC region of interest, the mean of the observers' measurements was adopted as the final value.

Cohen κ testing was used to evaluate the observer agreement for morphologic categories, and the majority opinion of the raters was designated the final value. If three opinions differed, it was resolved in consensus.

The relation between ADC and glioma subtypes was analyzed by using nonparametric testing (Kruskal-Wallis analysis of variance), including Dunn pairwise comparisons with Bonferroni correction. The strength of the association between glioma subtype and ADC metrics was probed by using Eta^2 (η^2). Eta^2 quantifies the percentage of variance in the dependent variable (ADC value) that is explained by one or more independent variables (glioma subtype).

Univariable logistic regression was applied to test if ADC metrics, age, or morphologic criteria could predict IDH^{wt} status. Nagelkerke (Pseudo) R^2 was used as a summary statistic expressing the degree to which the overall model predicts the variation in the outcome (IDH^{wt} status). Youden index was used to identify a diagnostic threshold for the most predictive (by area under the receiver operating characteristic curve [AUC] and R^2) ADC parameter. Morphologic categories with κ values of 0.6 or greater were subjected to univariable analysis. If significant ($P < .05$) at univariable analysis, features with substantial agreement (intraclass correlation coefficient > 0.8; κ > 0.6) were tested as predictor variables in a multivariable binomial logistic regression to predict glioma IDH^{wt} versus IDH^{mut} status. Starting from the highest P value, a backward elimination process by using the likelihood ratio test was applied to discard features that did not contribute significantly to the prediction, concluding with the most parsimonious model to identify *IDH* status. By the same method, an additional backward elimination was performed to develop an alternative model, into which

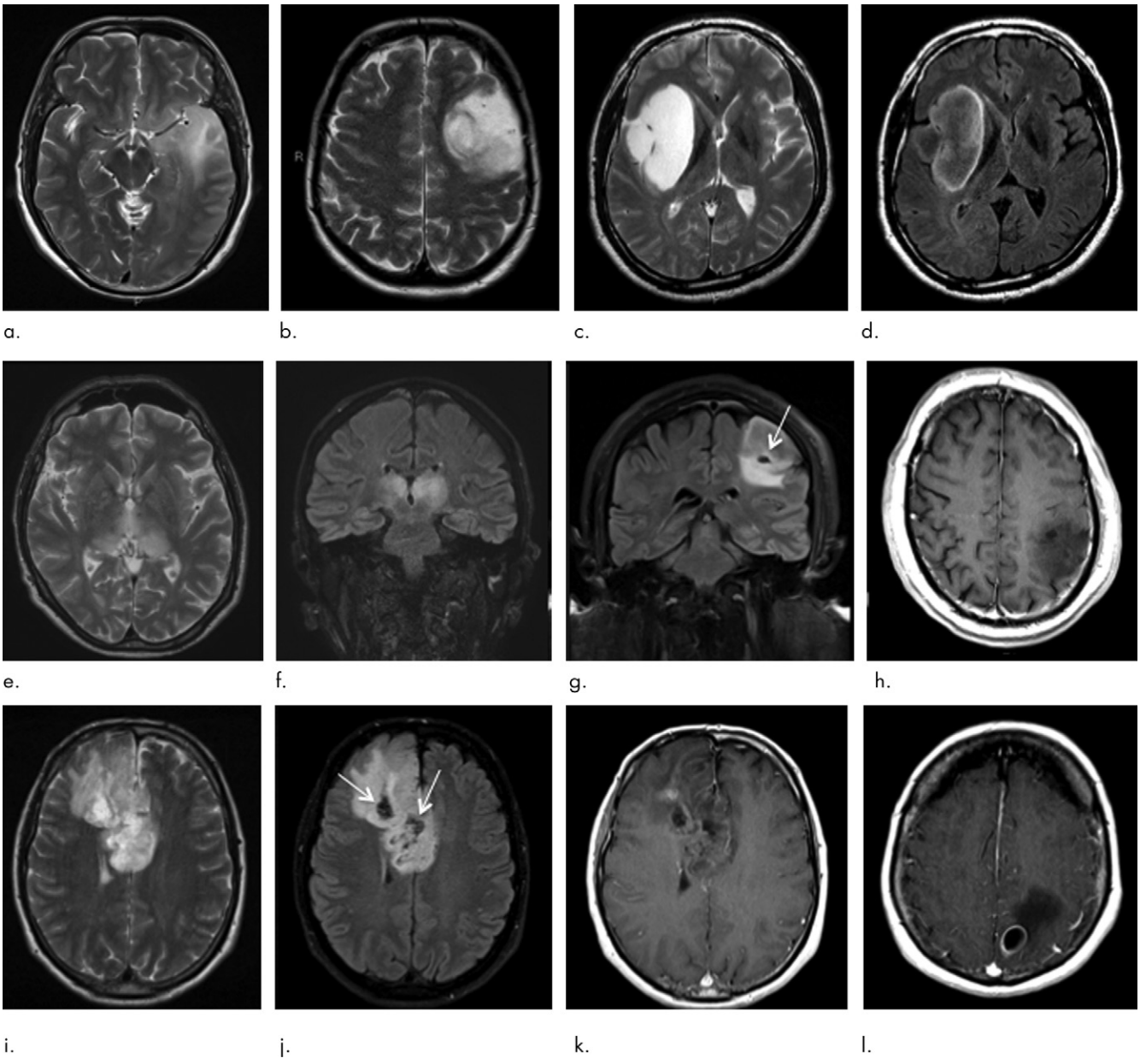

Figure 2: Glioma morphologic characteristics. **(a, b)** T2-weighted images show a temporal isocitrate dehydrogenase (*IDH*) wild-type (IDH^{wt}) glioma (**a**) versus another patient with a frontal *IDH* mutant (IDH^{mut})/*1p19q* codeleted ($1p19q^{del}$) glioma (**b**). Nonenhancing tumor margins: **(c, d)** T2-weighted and fluid-attenuated inversion recovery (FLAIR) images show distinct borders (also a T2-FLAIR mismatch sign) in an IDH^{mut}/*1p19q* intact (IDH^{mut}/$1p19q^{int}$) glioma versus **(e, f)** the indistinct margin of a bithalamic IDH^{wt} glioma. Cyst formation and enhancement patterns: **(g, h)** IDH^{mut}/$1p19q^{int}$ astrocytoma show a small cyst (arrow in **g**) nearly isointense to cerebrospinal fluid on FLAIR image without contrast agent uptake; **(i–k)** T2-weighted, FLAIR, and contrast-enhanced T1-weighted images show small cysts (arrows in **j**) and patchy contrast uptake in a IDH^{mut} $1p19q^{del}$ oligodendroglioma; **(l)** contrast-enhanced T1-weighted image shows rim enhancement surrounding central necrosis in an IDH^{wt} glioma.

calcification status was not entered, to allow for the clinical situation in which this may be unavailable from the existing imaging (eg, no CT and no T2*/susceptibility-weighted imaging performed). To assess model discrimination, we used a receiver operating characteristic analysis for both final models.

The numerical results from the multivariable regression developed with the study sample (n = 290) were then transcribed into a spreadsheet (Microsoft Excel for Mac version 14.5.2; Microsoft, Redmond, Wash) formula to calculate the IDH^{wt} status probability for individual patients with glioma in the subsequent test sample (n = 49) of previously unseen gliomas.

Results

Patient Demographics

At the start of the study, 515 patients were eligible for inclusion. After removal of duplicates (n = 42), 183 patients were excluded because of previous treatment for glioma (n = 60), tumor other than WHO grade II/III glioma (n = 43, and one cord tumor), ambiguous molecular result (n = 29), no preoperative diffusion-weighted imaging (n = 24, and 15 ADC map not computable), missing histopathologic report (n = 2), prolonged (≥1 year)

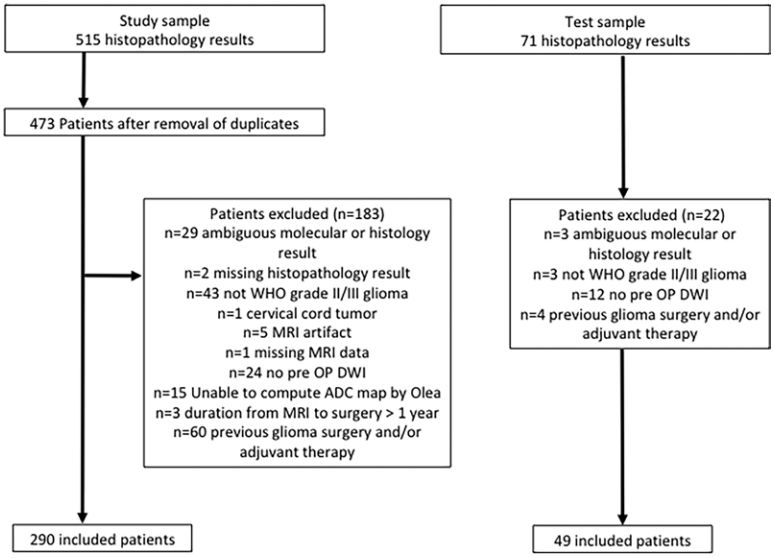

Figure 3: Patient selection flowchart. ADC = apparent diffusion coefficient, DWI = diffusion-weighted imaging, OP = operation, WHO = World Health Organization.

interval from MRI to operation (n = 3), or missing images (n = 1). A total of 290 patients (median age, 40 years; interquartile range, 33–52 years; 169 male patients) were included in the analysis of the study sample (patient inclusion from June 2008 to January 2018). An overview of the case selection process is in Figure 3. An overview of patient demographics and molecular groups is in Table 1. The relation between glioma *IDH* status and age was found to be nonlinear, with an exponential rise in the likelihood of IDH^{wt} status toward older age.

ADC Quantification for Glioma Molecular Subtyping

The interobserver reproducibility was good to excellent for all ADC parameters (intraclass correlation coefficient, 0.83–0.96). Consistency and absolute agreement were identical, indicating no systematic difference between the raters. Detailed intraclass correlation coefficient test results are shown in Table E2 (online). Each of the ADC parameters enabled IDH^{mut}/$1p19q^{del}$, IDH^{mut}/$1p19q^{int}$, and IDH^{wt} glioma discrimination ($P < .01$; Table E3, Fig E1 [online]).

Eta^2 (η^2) testing revealed an association between ADC values and glioma subtype for nongadolinium-enhancing and solidly enhancing tumors (η^2 = 0.28–0.42), but not for rim-enhanced masses (η^2 = 0–0.3) (Table E4 [online]). Across all gliomas, an ADC_{mean}-to-ADC_{NAWM} ratio of 1.8 predicted *IDH* status with a sensitivity of 69 of 79 (87%) and specificity of 124 of 208 (60%). For unenhanced gliomas, an ADC_{mean}-to-ADC_{NAWM} ratio threshold of 1.8 yielded a sensitivity of 28 of 33 (85%) and specificity of 93 of 140 (66%) for IDH^{wt} identification, compared with a sensitivity of 32 of 33 (97%) and specificity of 76 of 140 (54%) for a higher ADC_{mean}-to-ADC_{NAWM} ratio threshold of 1.9 (Fig 4).

Morphologic Assessment

For tumor location, the agreement between the three observers was good (κ = 0.81–0.89; $P < .001$; Table E5 [online]). Measurement of the single longest tumor diameter (<6 cm or ≥6 cm) demonstrated good agreement (κ = 0.80–0.82; $P \leq .001$). Defining calcification as present reached substantial agreement (κ = 0.67–0.74; $P \leq .001$) with uncertain results (eg, missing sequences) excluded. In 63.4% (184 of 290) of patients, one of three raters marked calcification as uncertain. In 11.7% (34 of 290), more than one rater specified calcification status as uncertain. The opinion of the raters regarding tumor cysts showed substantial agreement (κ = 0.66–0.70; $P \leq .001$). The categorization of enhancement patterns yielded substantial agreement (weighted κ = 0.69–0.77; $P \leq .001$).

Moderate interobserver agreement was found for unenhanced tumor margin (weighted κ = 0.45–0.61; $P \leq .001$) and for the T2-weighted FLAIR mismatch sign (κ = 0.44–0.62; $P < .001$). Fair agreement was observed for multifocality (κ = 0.20–0.46; $P < .001$) and hemorrhage (κ = 0.29–0.51; $P < .001$).

Univariable Analysis

The univariable logistic regression results are in Table 2 and Table E6 (online). Several features were statistically significant predictors, including all four ADC metrics (negative association), age (negative association), and several morphologic categories (enhancement pattern, nonenhancing margin, calcification, and cysts). ADC_{mean}-to-ADC_{NAWM} ratio was deemed the best-performing ADC parameter (AUC, 0.83; R^2 = 0.38). For the remaining diffusion parameters, the AUC values were marginally lower (AUCs: ADC_{min}, 0.78; ADC_{min}-to-ADC_{NAWM} ratio, 0.8; and ADC_{mean}, 0.81). Locations were grouped according to whether less than one-third, one- to two-thirds, or more than two-thirds of tumors represented IDH^{wt} gliomas to reduce the number of variables for statistical analysis. The presence of calcification was positively associated (odds ratio, 2.2; $P < .001$) with $1p19q^{del}$ status in IDH^{mut} gliomas (not tabulated). Tumor diameter and T2-FLAIR mismatch sign demonstrated no association with *IDH* status.

Multivariable Logistic Regression Model

The multivariable regression results are listed in Table 2 and Figure 5. The best-performing model (model A) for predicting IDH^{wt} (n = 82) versus IDH^{mut} (n = 208; 107 IDH^{mut}/$1p19q^{int}$ and 101 *IDH* IDH^{mut}/$1p19q^{del}$) genotype consisted of ADC_{mean}-to-ADC_{NAWM} ratio, age in years + age^2 (joint term), enhancement pattern, tumor location category (three groups: frontal or insula region, thalamus or brainstem, or elsewhere), and absence of calcification. On the basis of a likelihood cutoff value of 0.5 (50%), model A correctly classified 231 of 252 (91.6%; 95% confidence interval [CI]: 88%, 95%) gliomas, with an AUC of 0.96 (95% CI: 0.93, 0.98). In developing this model A, 38 of 290 (13.1%) patients were excluded by the statistics software; 33 patients were excluded because of uncertain calcification status as per the majority result of the raters, three patients were excluded because of absent ADC ratio values from tumor infiltration of normal-appearing white matter, one patient was excluded because of absent contrast

Table 1: Patient Demographics

Parameter	All Glioma Subtypes	IDH^{wt}	$IDH^{mut}/1p19q^{int}$	$IDH^{mut}/1p19q^{del}$
No. of patients	290	82	107*	101
Median age (y)	40 (17–77) [33–52]	58.50 (20–77) [24.25]	35 (17–66) [13]	40 (19–76) [13.50]
Enhancement category				
Nonenhancing	174	34	77	63
Patchy enhancing	89	28	28	33
Rim enhancing	25	20	0	5
Tumor location category				
Front or insula†	163	24	69	70
Other‡	113	45	37	31
Thalamus or brainstem§	14	13	1	0
Absence of calcification‖				
Noncalcified	225	70	94	61
Calcified	31	4	4	23
Absence of cyst or cysts				
Noncystic	189	73	58	58
Cystic	101	9	49	43
Hemorrhage#				
None	238	63	96	79
Petechial	7	5	2	0
Macroscopic	11	5	2	4
T2-weighted FLAIR mismatch				
Present	51	0	46	5
Absent	239	82	61	96
Diameter**				
≥6 cm	121	32	47	42
<6 cm	162	43	60	59

Note.—The study sample included 290 patients (169 men and 121 women). Data in parentheses are range and data in brackets are interquartile range. FLAIR = fluid-attenuated inversion recovery, *IDH* = isocitrate dehydrogenase, IDH^{wt} = *IDH* wild type, $IDH^{mut}/1p19q^{int}$ = *IDH* mutant and *1p19q* intact, $IDH^{mut}/1p19q^{del}$ = IDH mutant with synchronous deletion of the short arm of chromosome 1 and long arm of chromosome 19, IQR = interquartile range.

* Two patients within the IDH^{mut}/1p19q^{int} group had no postcontrast imaging available for assessment.

† The lesion was located in the frontal lobe or the insula.

‡ The lesion was in a location other than the frontal lobe, insula, thalamus, or brainstem.

§ The lesion was located in the thalamus or the brainstem.

‖ Calcification status was evaluated as uncertain in a total of 34 patients.

Hemorrhage status was evaluated as uncertain in a total of 34 patients.

** Single largest tumor diameter could not be clearly measured in a total of seven patients.

agent administration, and one patient was excluded because of both absent contrast agent administration and uncertain calcification status.

An alternative model (model B), derived by the same backward elimination method (except for not considering calcification status), performed nearly as well, achieving a correct classification of *IDH* status in 259 of 285 (90.9%; 95% CI: 88%, 94%) gliomas (AUC, 0.94; 95% CI: 0.93, 0.98). In the design of model B, the variable *no_calcification* was intentionally not entered to replicate the clinical situation where this information might be unavailable. Model B consisted of ADC_{mean}-to-ADC_{NAWM} ratio, age in years + age^2 (joint term), enhancement pattern, tumor location category, and absence of tumor cyst or cysts. For additional details on the logistic regression analysis, please see Table E6 (online). The diagnostic contribution from age and tumor morphologic structure is in Figures 6 and 7.

Test Sample

The numerical results from the study sample were transcribed into a software formula (Microsoft Excel for Mac version 14.5.2, Microsoft; see Note in Table 2) to calculate the IDH^{wt} status probability for individual patients with glioma in the subsequent test sample.

In the sample of patients with newly diagnosed glioma (n = 49; nine patients with IDH^{wt}, 21 patients with $IDH^{mut}/1p19q^{int}$, and 19 patients with $IDH^{mut}/1p19q^{del}$), the single blinded rater (A.A.B.) replicated the method of the main study. In cases of uncertainty regarding calcification (n = 5), the term *no calcification* was specified to permit results calculation.

Model A correctly classified *IDH* mutational status in 40 of 49 gliomas (82%; 95% CI: 71%, 93%), with 89% sensitivity and 80% specificity. Model B predicted *IDH* status in 42 of 49 (86%; 95% CI: 76%, 96%) gliomas, with a lower sensitivity of 67% but greater specificity of 90%.

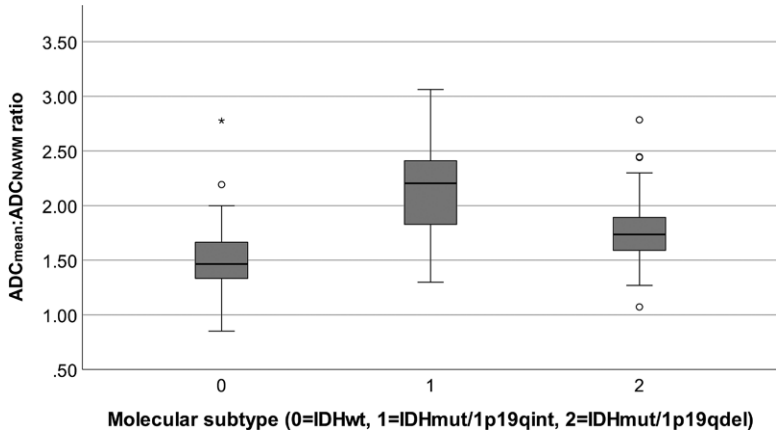

Figure 4: Boxplot shows differences in the apparent diffusion coefficient (ADC) values (mean ADC [ADC_{mean}]-to−normal-appearing white matter ADC [ADC_{NAWM}] ratio) between World Health Organization grade II/III glioma molecular subtypes in the study sample (82 wild-type isocitrate dehydrogenase [*IDH*; *IDH*wt]; 208 *IDH* mutation [*IDH*mut; 107 *IDH*mut/*1p19q*int, and 101 *IDH*mut/*1p19q*del).

Table 2: Univariable and Multivariable Binomial Logistic Regression Results for Prediction of Glioma *IDH*^{wt} Status in the Study Sample versus *IDH*^{mut}/1p19q^{int} or *IDH*^{mut}/1p19q^{del}

	Univariable Analyses		Multivariable Model A		Multivariable Model B	
Parameter	β Level	*P* Value	β Level	*P* Value	β Level	*P* Value
ADC_{mean}-to-ADC_{NAWM} ratio	−4.4	<.001	−5.7 (−8.1, −3.4)	<.001	−3.2 (−4.9, −1.6)	<.001
Age (y)	.09	<.001	−.05 (−.31, .21)	.71*	−.1 (−.3, .11)	.37*
Age^2 (y)	.01	<.001	.002 (.04 · 10^{-3}, .004)	.21*	.002 (.04 · 10^{-3}, .004)	.09*
Enhancement (categorical)						
Nonenhancing	Ref	Ref	Ref	Ref	Ref	Ref
Patchy enhancing	.64	.03	−.32 (−1.44, .81)	.58	−.41 (−1.4, .6)	.4
Rim enhancing	2.8	<.001	2.96 (.57, 5.34)	.02	1.7 (.3, 3.1)	.02
Tumor location category						
Front or insula†	Ref	Ref	Ref	Ref	Ref	Ref
Other‡	1.3	<.001	.78 (−.21, 1.76)	.12	.9 (.05, 1.7)	.04
Thalamus or brainstem§	4.3	<.001	3.6 (.9, 6.3)	.01	3.6 (1.3, 6.0)	.002
Absence of calcification	1.1	.045	4.3 (2.01, 6.7)	<.001	NA	
Absence of cyst(s)	1.9	<.001	NA		1.2 (.2, 2.2)	.02
Constant	NA		2.2 (−4.9, 9.4)	.54	3.1 (−2.8, 9.0)	.31
R^2	NA		.75		.65	

Note.—Data in parentheses are 95% confidence intervals. Numbers were rounded by one digit for publication. There were 82 patients in the study sample, 107 patients in the *IDH*^{mut}/1p10q^{int} group, and 101 patients in the *IDH*^{mut}/1p19q^{del} group. By using the multivariable regression results, a formula was designed to calculate the likelihood of wild-type isocitrate dehydrogenase (*IDH*) status for individual patients with glioma. The log odds ratios for models A and B are as follows: [L_A = (−5.71 × ADC_{mean}-to-ADC_{NAWM} ratio) + (−0.05 × age) + (0.002 × age^2) + (−0.32 × solid contrast enhancement) + (2.96 × rim contrast enhancement) + (0.78 × tumor location = other) + (3.58 × tumor location in thalamus or brainstem) + (4.34 × absent calcification) + 2.24] and [L_B = (-3.23 × ADC_{mean}-to-ADC_{NAWM} ratio) + (−0.1 × age) + (0.002 × age^2) + (−0.41 × solid contrast enhancement) + (1.66 × rim contrast enhancement) + (0.86 × tumor location = other) + (3.64 × tumor location in thalamus or brainstem) + (1.17 × absent cyst or cysts) + 3.07], respectively, where *solid contrast enhancement* and *rim contrast enhancement* pattern is 1 if present, 0 if absent, with each tumor assigned to one contrast enhancement category only; *tumor location* is 1 if in this category, 0 if not in this category; and *calcification* (model A)/cyst or cysts (model B) is 1 if present, 0 if absent (note the reversal is intentional). The probability of *IDH*^{wt} was calculated for models A and B by using the following equation: $1/(1 + e^{-L})$, where L is the relevant log odds ratio. ADC = apparent diffusion coefficient, ADC_{mean} = mean ADC, ADC_{NAWM} = ADC of normal-appearing white matter, *IDH*^{mut} = *IDH* mutation, *IDH*^{wt} = wild-type *IDH*, NA = not applicable, Ref = reference category.

* Age and age^2 are considered joint terms, hence a joint significance test was applicable. This was significant at $P < .001$, which combined with the likelihood ratio test confirmed a significant contribution of age to the prediction model.

† Indicates that the lesion was in the frontal lobe or the insula.

‡ Indicates that the lesion was in a location other than the frontal, insula, thalamus, or brainstem.

§ Indicates that the lesion was located in the thalamus or the brainstem.

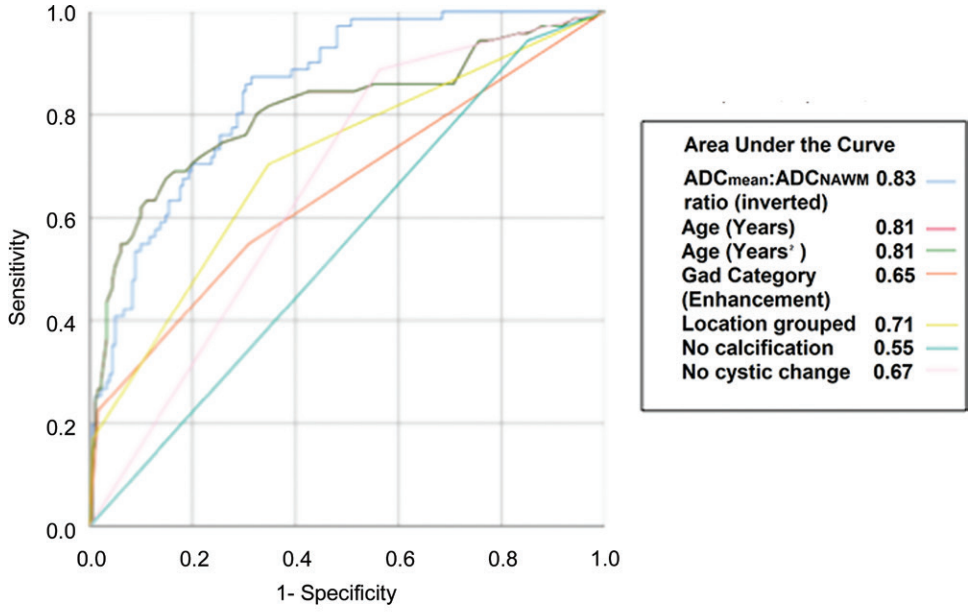

a.

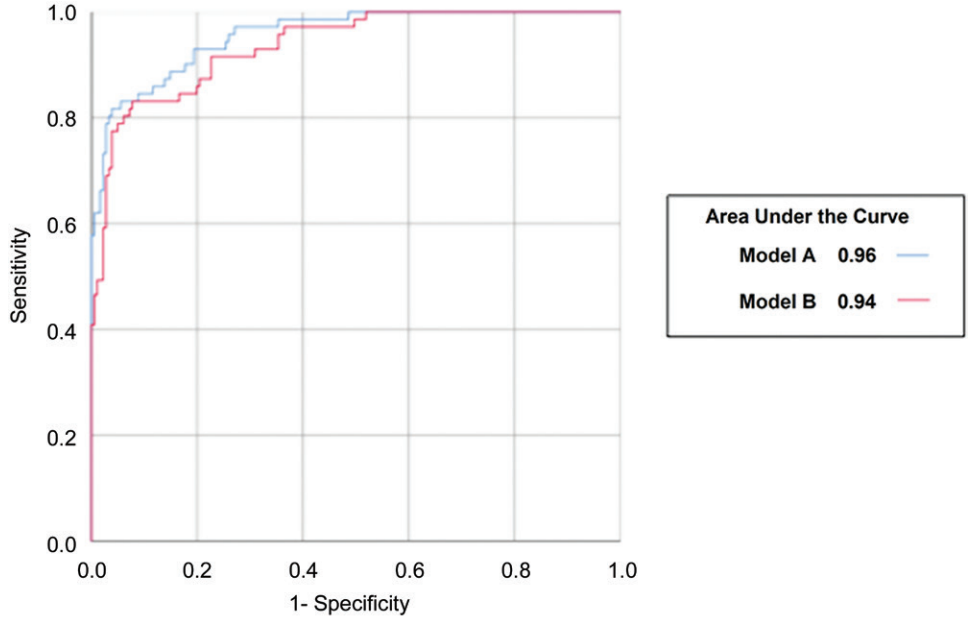

b.

Figure 5: Univariable and multivariable logistic regression analysis to predict isocitrate dehydrogenase (*IDH*) status in the study sample (82 wild-type *IDH* [IDH^{wt}] and 208 *IDH* mutation [IDH^{mut};107 $IDH^{mut}/1p19q^{int}$ and 101 $IDH^{mut}/1p19q^{del}$]). **(a)** Receiver operating characteristic curves show age and selected imaging features to predict (IDH^{wt}) glioma and **(b)** receiver operating characteristic curves of the multivariable probabilities for model A and B from Table 2 show similar model performance. Model A consisted of mean ADC (ADC_{mean})-to−ADC in normal-appearing white matter (ADC_{NAWM}) ratio, age in years + age^2 (joint term), enhancement pattern, tumor location category (three groups: frontal or insula region, thalamus or brainstem, or elsewhere), and absence of calcification. Model B consisted of ADC_{mean}-to-ADC_{NAWM} ratio, age in years + age^2 (joint term), enhancement pattern, tumor location category, and absence of tumor cyst or cysts.

Of the IDH^{mut} gliomas that were erroneously diagnosed as IDH^{wt} (eight gliomas by using model A and four gliomas by using model B), 75% (six of eight and three of four, respectively) were $IDH^{mut}/1p19q^{del}$ with an average ADC_{mean}-to-ADC_{NAWM} ratio of 1.43 (ranging from 1.21 to 1.76). One $IDH^{mut}/1p19q^{int}$ astrocytoma with an ADC_{mean}-to-ADC_{NAWM} ratio of 1.84 was misclassified by both models in an elderly patient (age, 81 years), and one anaplastic $IDH^{mut}/1p19q^{int}$ astrocytoma with an ADC_{mean}-to-ADC_{NAWM} ratio of 1.46 was misclassified by model A alone. The IDH^{wt} gliomas erroneously predicted as IDH^{mut} tumors (one of nine, model A; three of nine, model B) had ADC_{mean}-to-ADC_{NAWM} ratio values of 1.73–1.87. At subsequent review, all misclassified IDH^{wt} tumors exhibited a gliomatosis growth pattern with diffusely T2-weighted hyperintense infiltration of three or more lobes. In one IDH^{wt} glioma, the comparison ADC_{NAWM} ROI was sited in artifact (Nyquist ghost of scalp fat).

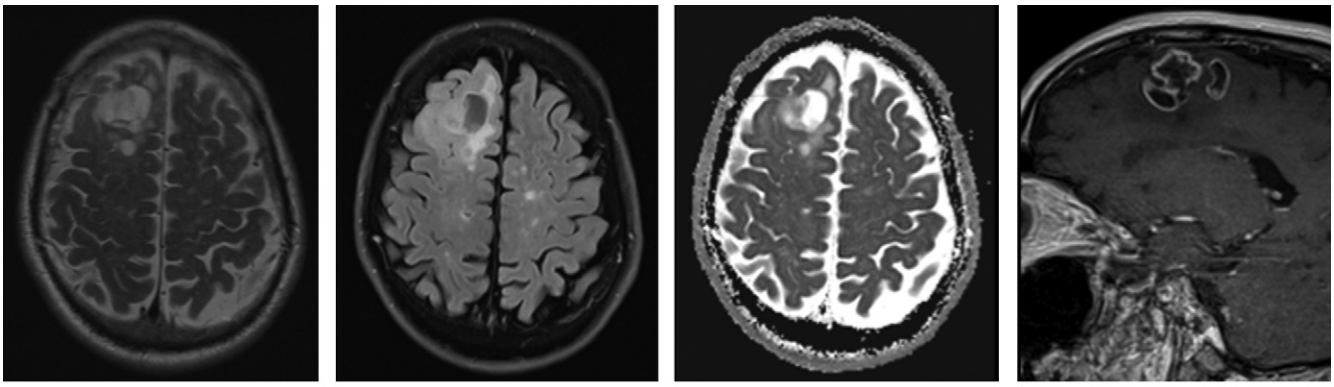

Figure 6: Images in a patient in whom the contribution of age and glioma morphologic structure resulted in correct isocitrate dehydrogenase (*IDH*) status classification over apparent diffusion coefficient alone. **(a)** T2-weighted, **(b)** fluid-attenuated inversion recovery, **(c)** apparent diffusion coefficient (ADC), and **(d)** T1-weighted gadolinium chelate—enhanced images in a male patient age 75 years with an *IDH* wild-type glioma tumor with high solid component diffusivity (mean ADC—to—ADC in normal-appearing white matter ratio, 2.19) and a rim-enhancement pattern.

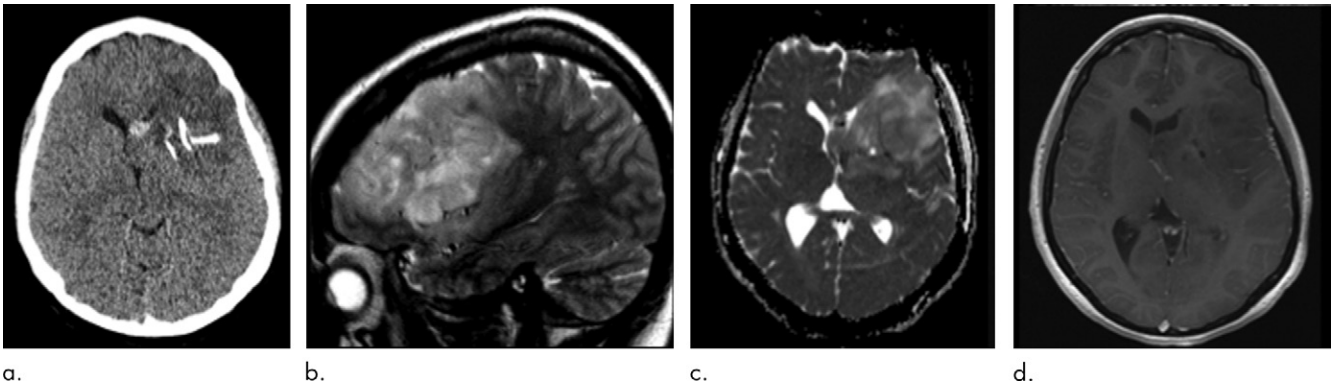

Figure 7: Images in a patient in whom the contribution of age and glioma morphologic structure resulted in correct isocitrate dehydrogenase (*IDH*) status classification over apparent diffusion coefficient (ADC) alone. **(a)** Noncontrast-enhanced CT, **(b)** T2-weighted, **(c)** ADC, and **(d)** T1-weighted gadolinium chelate—enhanced images in a male patient age 45 years with a calcified *IDH* mutant/1p19q codeleted oligodendroglioma (mean ADC—to—ADC in normal-appearing white matter ratio of 1.07).

Discussion

In this study, the combination of apparent diffusion coefficient (ADC) region of interest measurements (mean apparent diffusion coefficient [ADC; ADC_{mean}]-to–normal-appearing gray matter ADC [ADC_{NAWM}] ratio) and morphologic descriptors (enhancement, calcification, and cyst formation) measured at standard MRI (10) permitted isocitrate dehydrogenase (*IDH*) genotyping of lower-grade gliomas (area under the receiver operating characteristic curve [AUC], 0.94–0.96; study sample, 290 patients). Two models, model A (mandating calcification result) and model B (recording cyst formation), were developed, which correctly classified *IDH* status with similar accuracy (82% and 86%, respectively) in a previously unseen test sample ($n = 49$) of World Health Organization II/III gliomas. By using ADC values alone, significant differences were observed between *IDH* mutation (IDH^{mut})/$1p19q^{del}$, IDH^{mut}/$1p19q^{int}$, and *IDH* wild-type (IDH^{wt}) glioma subtypes ($P < .001$), but the *IDH* status prediction was less precise (AUC, 0.83 for ADC_{mean}-to-ADC_{NAWM} ratio).

Volumetric (12,14) and region-derived minimum (11) and mean (14) ADC measurements were previously used to estimate WHO grade II/III glioma IDH status. Our study confirms excellent (intraclass correlation coefficient, 0.83–0.96) interobserver agreement for ROI measurements, consistent with the reproducibility of ADC values described in other cancer research (21). Whereas ADC values are independent of hardware and field strength at fixed parameters (22), the use of a ratio offers the further advantage of being vendor neutral. Drawing one maximum-size round ADC_{mean} ROI in the largest tumor cross-section is considered feasible on most clinical workstations. Good reproducibility was shown previously for two observers by using ADC_{mean}-to-ADC_{NAWM} ratio regions of interest, representative of entire lesion volumetric measurements (14). In our analysis, three observers used the technique in the study sample, and one observer in the test sample, amounting to a total of six different observers between the studies. It is hypothesized that most lower-grade gliomas are sufficiently homogeneous to make such ROI measurements reliable.

When testing ADC_{mean}-to-ADC_{NAWM} ratio for *IDH* typing, we confirmed a threshold in the region of 1.8 (14), applicable to solid tumors with or without contrast enhancement. ADC values appear unreliable for *IDH* typing in rim-enhanced necrotic gliomas even when measured in macroscopically solid components, which mirrors a previous study (23) of WHO grade IV glioblastoma.

The accuracy of ADC_{mean}-to-ADC_{NAWM} ratio alone for predicting WHO II/III grade glioma *IDH* status in our study (AUC, 0.83 across all tumor morphologic characteristics) exceeded that of published approaches by using multishell diffusion (neurite orientation dispersion and density imaging; AUC maximum, 0.76) (24) and diffusion kurtosis (AUC maximum, 0.72 [25] and 0.79 [26]). The ADC_{mean}-to-ADC_{NAWM} ratio was a highly significant predictor ($P < .001$) in both multivariable models, indicating a strong inverse relationship between ADC and the likelihood of IDH^{wt} status.

Because the qualitative description of glioma features is subjective, we limited the statistical modeling to morphologic categories with substantial agreement such as tumor location. Frontal glioma location has repeatedly been associated with IDH^{mut} status (27,28). Gozé et al (29) found 100% of insula-centered low-grade gliomas to be IDH^{mut}. In our study, both locations were similarly associated with a greater likelihood of IDH^{mut} status, which is also consistent with a report by Xiong et al (30). Conversely, we confirmed that thalamic or brainstem location is predominantly a feature of IDH^{wt}, which may variably be associated with malignant glioma mutations such as *H3 K27M* (31).

In our study, the presence versus absence of solid enhancement was not consistently associated with IDH status (multivariable P = .41–.58). However, glioblastoma morphologic characteristics featuring rim enhancement was a predictor of IDH^{wt} status. We did not test percentage enhancement, which in a study by Delfanti et al (27) failed to predict *IDH* type.

The absence of calcification strongly correlated with IDH^{wt} status and negatively with $1p19q^{del}$ at univariable analysis. In a study by Kanazawa et al (18), both calcification and cysts were significantly related to $IDH^{mut}/1p19q^{del}$. We hypothesize that in many patients undergoing CT at diagnosis, consistent availability of this and/or susceptibility-weighted imaging could further increase observer certainty and concordance. In keeping with our observations (model B), absence of cysts has been proposed previously as an IDH^{wt} glioma feature (32).

In our study sample, there was no association between multifocality and *IDH* status, which was recently proposed as a feature predictive of IDH^{wt} in WHO grade II glioma (33). Our results support that the T2-FLAIR mismatch sign is a specific feature of $IDH^{mut}/1p19q^{int}$ status. However, the interobserver agreement was moderate (κ = 0.44–0.62), closer to the lower 95% CI bound (κ = 0.53) of the original publication by Patel et al (20). The T2-FLAIR mismatch sign did not directly predict *IDH* status because all molecular glioma subtypes can lack this feature. For nonenhancing margin definition, the agreement was moderate, meaning that although IDH^{wt} gliomas are less well demarcated (16,34), subjectivity and overlap with $IDH^{mut}/1p19q^{del}$ indistinct margins (35) limit the reproducibility of this feature.

Our study had some limitations, including its retrospective design and that it lacked a definitive calcification result in a proportion of patients. Both models may have a misclassification risk for low diffusivity $IDH^{mut}/1p19q^{del}$ oligodendrogliomas and for IDH^{wt} tumors exhibiting a T2-weighted and ADC hyperintense gliomatosis growth pattern. We have not tested the models on WHO grade IV gliomas.

In conclusion, the combination of mean apparent diffusion coefficient (ADC)-to–normal-appearing white matter ADC ratio, tumor morphologic characteristics, and age predicted the presence of isocitrate dehydrogenase (*IDH)* wild-type glioma versus *IDH* mutation tumor types with high accuracy.

Author contributions: Guarantors of integrity of entire study, J.M., S.T.; study concepts/study design or data acquisition or data analysis/interpretation, all authors; manuscript drafting or manuscript revision for important intellectual content, J.M., S.W., R.J., S.T.; approval of final version of submitted manuscript, all authors; agrees to ensure any questions related to the work are appropriately resolved, all authors; literature research, J.M., W.M., R.J., S.T.; clinical studies, J.M., S.O., A.A.B., W.M., S.B., A.M.K., R.J., S.T.; statistical analysis, J.M., S.W., O.A., S.T.; and manuscript editing, all authors

Disclosures of Conflicts of Interest: **J.M.** disclosed no relevant relationships. **S.O.** disclosed no relevant relationships. **S.W.** disclosed no relevant relationships. **A.A.B.** disclosed no relevant relationships. **O.A.** disclosed no relevant relationships. **W.M.** disclosed no relevant relationships. **S.B.** disclosed no relevant relationships. **Z.J.** disclosed no relevant relationships. **A.M.K.** disclosed no relevant relationships. **L.M.** disclosed no relevant relationships. **R.J.** disclosed no relevant relationships. **S.T.** disclosed no relevant relationships.

References

1. Eckel-Passow JE, Lachance DH, Molinaro AM, et al. Glioma Groups Based on 1p/19q, IDH, and TERT Promoter Mutations in Tumors. N Engl J Med 2015;372(26):2499–2508.
2. Stichel D, Ebrahimi A, Reuss D, et al. Distribution of EGFR amplification, combined chromosome 7 gain and chromosome 10 loss, and TERT promoter mutation in brain tumors and their potential for the reclassification of IDHwt astrocytoma to glioblastoma. Acta Neuropathol (Berl) 2018;136(5):793–803.
3. Louis DN, Perry A, Burger P, et al. International Society Of Neuropathology--Haarlem consensus guidelines for nervous system tumor classification and grading. Brain Pathol 2014;24(5):429–435.
4. Yan H, Parsons DW, Jin G, et al. IDH1 and IDH2 mutations in gliomas. N Engl J Med 2009;360(8):765–773.
5. Cancer Genome Atlas Research Network, Brat DJ, Verhaak RG, et al. Comprehensive, Integrative Genomic Analysis of Diffuse Lower-Grade Gliomas. N Engl J Med 2015;372(26):2481–2498.
6. van den Bent MJ, Brandes AA, Taphoorn MJB, et al. Adjuvant procarbazine, lomustine, and vincristine chemotherapy in newly diagnosed anaplastic oligodendroglioma: long-term follow-up of EORTC brain tumor group study 26951. J Clin Oncol 2013;31(3):344–350.
7. Kreth FW, Thon N, Simon M, et al. Gross total but not incomplete resection of glioblastoma prolongs survival in the era of radiochemotherapy. Ann Oncol 2013;24(12):3117–3123.
8. Li YM, Suki D, Hess K, Sawaya R. The influence of maximum safe resection of glioblastoma on survival in 1229 patients: Can we do better than gross-total resection? J Neurosurg 2016;124(4):977–988.
9. Patterson DM, Padhani AR, Collins DJ. Technology insight: water diffusion MRI--a potential new biomarker of response to cancer therapy. Nat Clin Pract Oncol 2008;5(4):220–233.
10. Thust SC, Heiland S, Falini A, et al. Glioma imaging in Europe: A survey of 220 centres and recommendations for best clinical practice. Eur Radiol 2018;28(8):3306–3317.
11. Xing Z, Yang X, She D, Lin Y, Zhang Y, Cao D. Noninvasive Assessment of *IDH* Mutational Status in World Health Organization Grade II and III Astrocytomas Using DWI and DSC-PWI Combined with Conventional MR Imaging. AJNR Am J Neuroradiol 2017;38(6):1138–1144.
12. Leu K, Ott GA, Lai A, et al. Perfusion and diffusion MRI signatures in histologic and genetic subtypes of WHO grade II-III diffuse gliomas. J Neurooncol 2017;134(1):177–188.
13. Hempel JM, Schittenhelm J, Brendle C, et al. Histogram analysis of diffusion kurtosis imaging estimates for in vivo assessment of 2016 WHO glioma grades: A cross-sectional observational study. Eur J Radiol 2017;95:202–211.
14. Thust SC, Hassanein S, Bisdas S, et al. Apparent diffusion coefficient for molecular subtyping of non-gadolinium-enhancing WHO grade II/III glioma: volumetric segmentation versus two-dimensional region of interest analysis. Eur Radiol 2018;28(9):3779–3788.
15. Juratli TA, Tummala SS, Riedl A, et al. Radiographic assessment of contrast enhancement and T2/FLAIR mismatch sign in lower grade gliomas: correlation with molecular groups. J Neurooncol 2019;141(2):327–335.

16. Zhou H, Vallières M, Bai HX, et al. MRI features predict survival and molecular markers in diffuse lower-grade gliomas. Neuro Oncol 2017;19(6):862–870.
17. Reuss DE, Sahm F, Schrimpf D, et al. ATRX and IDH1-R132H immunohistochemistry with subsequent copy number analysis and IDH sequencing as a basis for an "integrated" diagnostic approach for adult astrocytoma, oligodendroglioma and glioblastoma. Acta Neuropathol (Berl) 2015;129(1):133–146.
18. Kanazawa T, Fujiwara H, Takahashi H, et al. Imaging scoring systems for preoperative molecular diagnoses of lower-grade gliomas. Neurosurg Rev 2019;42(2):433–441.
19. Pignatti F, van den Bent M, Curran D, et al. Prognostic factors for survival in adult patients with cerebral low-grade glioma. J Clin Oncol 2002;20(8):2076–2084.
20. Patel SH, Poisson LM, Brat DJ, et al. T2-FLAIR Mismatch, an Imaging Biomarker for IDH and 1p/19q Status in Lower-grade Gliomas: A TCGA/TCIA Project. Clin Cancer Res 2017;23(20):6078–6085.
21. Newitt DC, Zhang Z, Gibbs JE, et al. Test-retest repeatability and reproducibility of ADC measures by breast DWI: Results from the ACRIN 6698 trial. J Magn Reson Imaging 2019;49(6):1617–1628.
22. Ogura A, Tamura T, Ozaki M, et al. Apparent Diffusion Coefficient Value Is Not Dependent on Magnetic Resonance Systems and Field Strength Under Fixed Imaging Parameters in Brain. J Comput Assist Tomogr 2015;39(5):760–765.
23. Tan WL, Huang WY, Yin B, Xiong J, Wu JS, Geng DY. Can diffusion tensor imaging noninvasively detect IDH1 gene mutations in astrogliomas? A retrospective study of 112 cases. AJNR Am J Neuroradiol 2014;35(5):920–927.
24. Figini M, Riva M, Graham M, et al. Prediction of Isocitrate Dehydrogenase Genotype in Brain Gliomas with MRI: Single-Shell versus Multishell Diffusion Models. Radiology 2018;289(3):788–796.
25. Zhao J, Wang YL, Li XB, et al. Comparative analysis of the diffusion kurtosis imaging and diffusion tensor imaging in grading gliomas, predicting tumour cell proliferation and IDH-1 gene mutation status. J Neurooncol 2019;141(1):195–203.
26. Tan Y, Zhang H, Wang X, et al. Comparing the value of DKI and DTI in detecting isocitrate dehydrogenase genotype of astrocytomas. Clin Radiol 2019;74(4):314–320.
27. Delfanti RL, Piccioni DE, Handwerker J, et al. Imaging correlates for the 2016 update on WHO classification of grade II/III gliomas: implications for IDH, 1p/19q and ATRX status. J Neurooncol 2017;135(3):601–609 [Published correction appears in J Neurooncol 2017;135(3):611.].
28. Sonoda Y, Shibahara I, Kawaguchi T, et al. Association between molecular alterations and tumor location and MRI characteristics in anaplastic gliomas. Brain Tumor Pathol 2015;32(2):99–104.
29. Gozé C, Mansour L, Rigau V, Duffau H. Distinct IDH1/IDH2 mutation profiles in purely insular versus paralimbic WHO Grade II gliomas. J Neurosurg 2013;118(4):866–872.
30. Xiong J, Tan W, Wen J, et al. Combination of diffusion tensor imaging and conventional MRI correlates with isocitrate dehydrogenase 1/2 mutations but not 1p/19q genotyping in oligodendroglial tumours. Eur Radiol 2016;26(6):1705–1715.
31. Reyes-Botero G, Giry M, Mokhtari K, et al. Molecular analysis of diffuse intrinsic brainstem gliomas in adults. J Neurooncol 2014;116(2):405–411.
32. Wu CC, Jain R, Radmanesh A, et al. Predicting Genotype and Survival in Glioma Using Standard Clinical MR Imaging Apparent Diffusion Coefficient Images: A Pilot Study from The Cancer Genome Atlas. AJNR Am J Neuroradiol 2018;39(10):1814–1820.
33. Villanueva-Meyer JE, Wood MD, Choi BS, et al. MRI Features and IDH Mutational Status of Grade II Diffuse Gliomas: Impact on Diagnosis and Prognosis. AJR Am J Roentgenol 2018;210(3):621–628.
34. Park YW, Han K, Ahn SS, et al. Prediction of *IDH1*-Mutation and 1p/19q-Codeletion Status Using Preoperative MR Imaging Phenotypes in Lower Grade Gliomas. AJNR Am J Neuroradiol 2018;39(1):37–42.
35. Johnson DR, Diehn FE, Giannini C, et al. Genetically Defined Oligodendroglioma Is Characterized by Indistinct Tumor Borders at MRI. AJNR Am J Neuroradiol 2017;38(4):678–684.